Electrocatalysis

International Edition: DOI: 10.1002/anie.201505307
German Edition: DOI: 10.1002/ange.201505307

Function-Led Design of Aerogels: Self-Assembly of Alloyed PdNi Hollow Nanospheres for Efficient Electrocatalysis

*Bin Cai, Dan Wen, Wei Liu, Anne-Kristin Herrmann, Albrecht Benad, and Alexander Eychmüller**

Abstract: *One plausible approach to endow aerogels with specific properties while preserving their other attributes is to fine-tune the building blocks. However, the preparation of metallic aerogels with designated properties, for example catalytically beneficial morphologies and transition-metal doping, still remains a challenge. Here, we report on the first aerogel electrocatalyst composed entirely of alloyed PdNi hollow nanospheres (HNSs) with controllable chemical composition and shell thickness. The combination of transition-metal doping, hollow building blocks, and the three-dimensional network structure make the PdNi HNS aerogels promising electrocatalysts for ethanol oxidation. The mass activity of the $Pd_{83}Ni_{17}$ HNS aerogel is 5.6-fold higher than that of the commercial Pd/C catalyst. This work expands the exploitation of the electrocatalysis properties of aerogels through the morphology and composition control of its building blocks.*

Assemblies of nanomaterials in the form of macroscopic aerogel frameworks have attracted great interest in the nanotechnology revolution due to their extremely high porosity and large specific surface area.[1] Since the pioneering work on aerogels in the early 1930s, different inorganic and organic building blocks have been employed to explore potential applications.[2] For instance, Leventis et al. reported metallic aerogels (from non-noble metals, including Fe, Co, Cu) made by a carbothermal method.[3] Brock et al. made exceptional contributions to the development of semiconductor- and quantum-dot-derived aerogels.[4] Arachchige et al. expanded Ag-based metallic aerogels into controlled morphologies.[5] Meanwhile, our group has reported on a series of pure and mixed aerogels (made of noble metals, semiconductors, and quantum dots).[6] The aerogels reported up to now have shown great application potential in the areas of catalysis, energy storage, and thermoresistors.[7] However, the applications of these aerogels, in particular the metal-based aerogels, lag far behind the plethora of preparations.[8]

Metallic aerogels combine the advantages of metals and aerogels, such as the metallic backbone (enables rapid electron transfer), large surface area (provides more reactive sites), high porosity (accelerates mass transfer), and self-supportability (eliminates support corrosion), which unleashed tremendous potential in electrocatalysis.[9] Nonetheless, the investigation of metallic aerogel electrocatalysts is still in the early stages and is largely limited by the solid building blocks.[7] The previous reports have shown that the intimate relationship between the nanocomponents and the macro-aerogel provides a straightforward modality for the deliberate tailoring of aerogel properties by optimization of the building blocks. Thus, it is of great interest to endow aerogel catalysts with new properties by optimizing the nano building blocks. For noble-metal electrocatalysts, regulation of the morphology and alloying with transition metals remain the most efficient ways to meet the industrial requirements.[10] Despite the recent reports on the electrocatalytic and bioelectrocatalytic activities of pure Pd and PdPt metallic aerogels,[9] the design of efficient aerogel electrocatalysts based on catalytically beneficial morphologies and transition-metal doping has not been reported to date.

In this context, bimetallic aerogels composed entirely of alloyed PdNi hollow nanospheres (HNSs) were prepared by a facile bottom-up method. The PdNi HNS building blocks connect and fuse into a well-defined three-dimensional (3D) necklace-like network structure during the gelation process. It has been demonstrated that nanocrystals with a hollow interior exhibit better catalytic activities than their solid counterparts. Since its electronic properties can be manipulated, nickel is an ideal transition metal for optimizing the potential of the noble metal.[11]

As shown in Scheme 1, the alloyed PdNi HNSs which serve as the building blocks (with a diameter of ca. 30 nm and shell thickness of ca. 5 nm) were synthesized via a galvanic replacement method using Ni nanoparticles (NPs) as sacrificial templates (Figure S1). Since aqueous solutions of the HNSs are normally very stable in the as-prepared state, it is necessary to concentrate the sols and eliminate parts of the stabilizers to reach a "metastable state." (The highly concentrated sols are still very stable after two months.[6a]) The gelation process was achieved by heating the concentrated sols at 348 K for 6 h. After the solvent of the resulting hydrogels had been exchanged with acetone and the pore liquid evaporated using supercritical drying, self-supported monolithic HNS aerogels were obtained (Figure S2).

As shown in the scanning electron microscopy (SEM) and transmission electron microscopy (TEM) images (Figure 1 a–c and Figure S3), the PdNi HNS aerogel has an excellent 3D porous network structure arising from the fusion and random interconnection of individual HNSs. The necklace-like backbone has the same diameter (ca. 30 nm) as its HNS building

[*] B. Cai, Dr. D. Wen, Dr. W. Liu, Dr. A.-K. Herrmann, A. Benad, Prof. A. Eychmüller
Physikalische Chemie, TU Dresden
Bergstrasse 66b, 01062 Dresden (Germany)
E-mail: alexander.eychmueller@chemie.tu-dresden.de
Homepage: http://www.chm.tu-dresden.de/pc2/

Supporting information for this article is available on the WWW under http://dx.doi.org/10.1002/anie.201505307.

 © 2015 Wiley-VCH Verlag GmbH & Co. KGaA, Weinheim

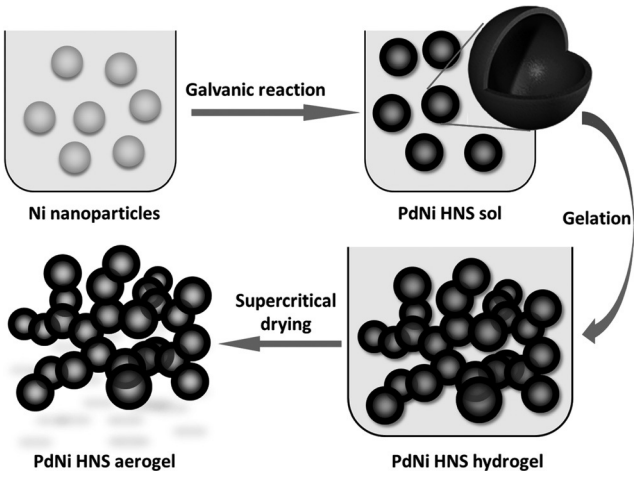

Scheme 1. Illustration of the synthesis procedure.

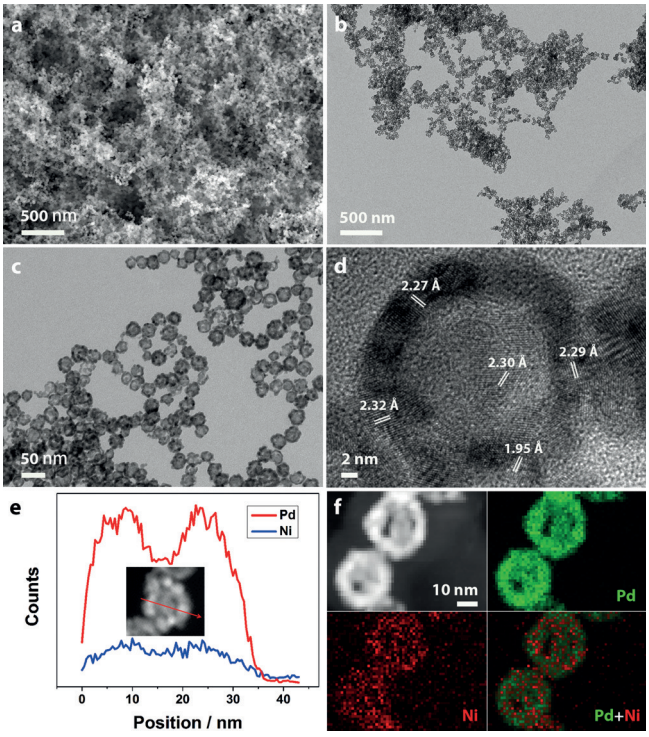

Figure 1. a) SEM and b,c) TEM images of the $Pd_{83}Ni_{17}$ HNS aerogel at different magnifications. d) HR-TEM characterization of the fused connection and an HNS area of the $Pd_{83}Ni_{17}$ HNS aerogel. e) STEM-EDX line-scanning profile and f) high-angle annular dark field (HAADF) STEM imaging and elemental mapping analysis of Pd and Ni.

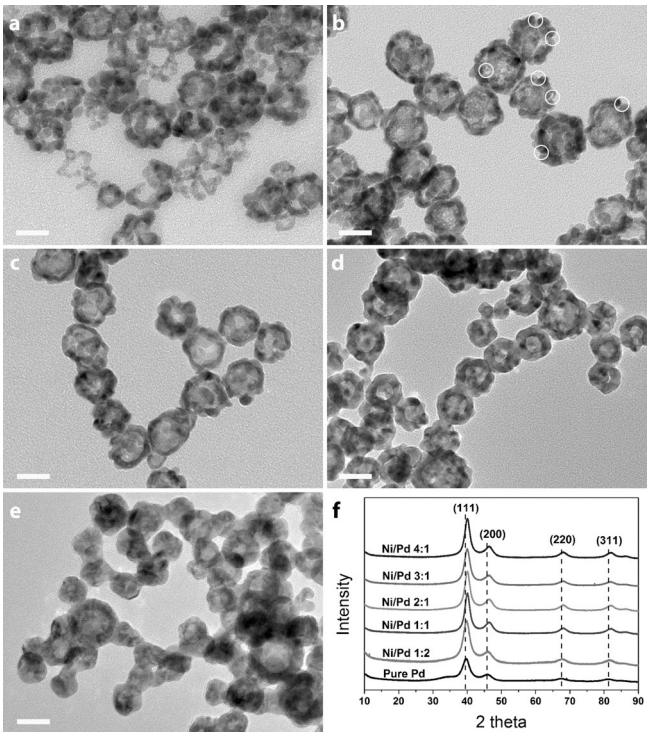

Figure 2. TEM images of Pd_xNi_y HNS aerogels with different Ni/Pd precursor ratios: a) 4:1, b) 3:1, c) 2:1, d) 1:1, and e) 1:2. Scale bar is 20 nm. f) XRD analysis of Pd_xNi_y HNS aerogels with different Ni/Pd precursor ratios.

blocks, indicating the HNSs remain intact during the gelation and drying processes. The crystalline properties of the HNSs and their fused junction area were demonstrated by high-resolution TEM (HR-TEM) images (Figure 1 d and Figure S4). The regular face-centered-cubic (fcc) lattice is observed throughout the "necklace" region. Lattice spacings of about 2.30 Å, which can be indexed to the (111) planes, are widely distributed at all locations. The crystalline properties were further examined by X-ray diffraction (XRD) (Figure 2 f), which shows that all the four characteristic peaks of the PdNi alloy are shifted towards larger diffraction angles, suggesting a lattice contraction with increasing Ni content.[12] The slight shrinkage of the lattice parameters relative to those of our previous pure Pd aerogel can be explained by the permeation of Ni atoms into the Pd lattice which results in smaller crystallographic unit cells.[6b,13] Figure 1 e,f show the STEM energy-dispersive X-ray (STEM-EDX) line-scanning profiling and elemental mapping analysis, respectively. Here, Pd and Ni are both distributed throughout the HNSs and the signals in the shell area are stronger than in the core area, which reflects the formation of the PdNi alloy and the hollow structure. X-ray photoelectron spectroscopy (XPS) was further employed to investigate the electronic environment of Pd and Ni in the HNS aerogel structure (Figure S5). Summarizing the EDX, XPS, and ICP-OES analyses (see the Supporting Information), the Pd/Ni molar ratio of the alloyed HNS aerogel is 83:17, and it can be denoted as $Pd_{83}Ni_{17}$ HNS aerogel.

The physicochemical properties, including the electrocatalytic activities, of bimetallic nanoarchitectures are known to be highly dependent on the elemental composition.[14] Thus we used different amounts of Pd precursors in order to tune the composition of the resulting PdNi HNS aerogels. The Ni content of the HNS aerogels ranges from 3 to 19%, as the molar ratio of the Ni/Pd precursors varies from 1:2 to 4:1 (Figure S6). The TEM images in Figure 2 present the increasing shell thickness and the decreasing diameter with

© 2015 Wiley-VCH Verlag GmbH & Co. KGaA, Weinheim

the decrease of the Ni/Pd ratio. When the Ni/Pd ratio decreases to 1:2, the thickness of the shells and the diameters are reduced to ca. 7 and 23 nm, respectively; the HNSs display a shrunken hollow interior and a more fused network structure. Conversely, more broken HNSs and smaller shell fragments are observed in the aerogel structure when the Ni/Pd ratio reaches 4:1. Thus, the Ni/Pd ratio of 3:1 ($Pd_{83}Ni_{17}$) is most suitable for realizing the thinnest shell while keeping the structure intact. The XRD analysis (Figure 2 f) demonstrates that the Pd_xNi_y HNS aerogels share the same fcc crystalline structure regardless of the compositional change. The increased asymmetry of the diffraction peaks with an increased in Ni content implies the incorporation of Ni atoms into the Pd lattice.[15]

Taking the $Pd_{83}Ni_{17}$ HNS aerogel as an example, the surface area and porosity were further evaluated based on the N_2 physisorption isotherms (Figure S7). The adsorption isotherm combines the characteristics of type II and type IV isotherms, which indicates the wide spread of both meso- and macropores within the aerogel structure. As estimated from a Brunauer–Emmett–Teller (BET) plot, the surface area is 95.4 $m^2 g^{-1}$, which is in the range of that of noble-metal nanoparticle-based aerogels (32–168 $m^2 g^{-1}$).[7] The pore size distribution analysis exhibits a distinct pore distribution peak at ca. 22 nm which is attributed to the hollow cavity of the building blocks. The density of the $Pd_{83}Ni_{17}$ HNS aerogel is estimated to be 0.035 $g cm^{-3}$, which further indicates the high porosity.

It is reasonable to anticipate that the HNS aerogels are electrochemically more accessible due to the combination of their hollow structure and the 3D network assembly. As shown in Figure 3 a and Figure S8, cyclic voltammograms (CVs) of Pd_xNi_y HNS aerogels and Pd/C-modified electrodes were obtained in 1 M NaOH solution. Their electrochemical active surface area (ECSA) values were estimated by employing the reduction charge of Pd oxide and assuming a charge density of 430 $\mu C cm^{-2}$ for the formation of a PdO monolayer.[16] The Pd_xNi_y HNS aerogels exhibit different ECSA values (56.9, 55.5, 54.7, 51.1, and 47.8 $m^2 g^{-1}$ with the Ni content ranging from 19 % to 3 %), while the ECSA value of Pd/C is 42.3 $m^2 g^{-1}$. Even more convincingly, the ECSA value of the $Pd_{83}Ni_{17}$ HNS building blocks is 45.2 $m^2 g^{-1}$, 1.23 times lower than that of their aerogel counterparts, indicating the significance of the aerogel structure in the preservation of ECSA. The higher ECSA values indicate that more active sites are accessible, suggesting an increase in the utilization

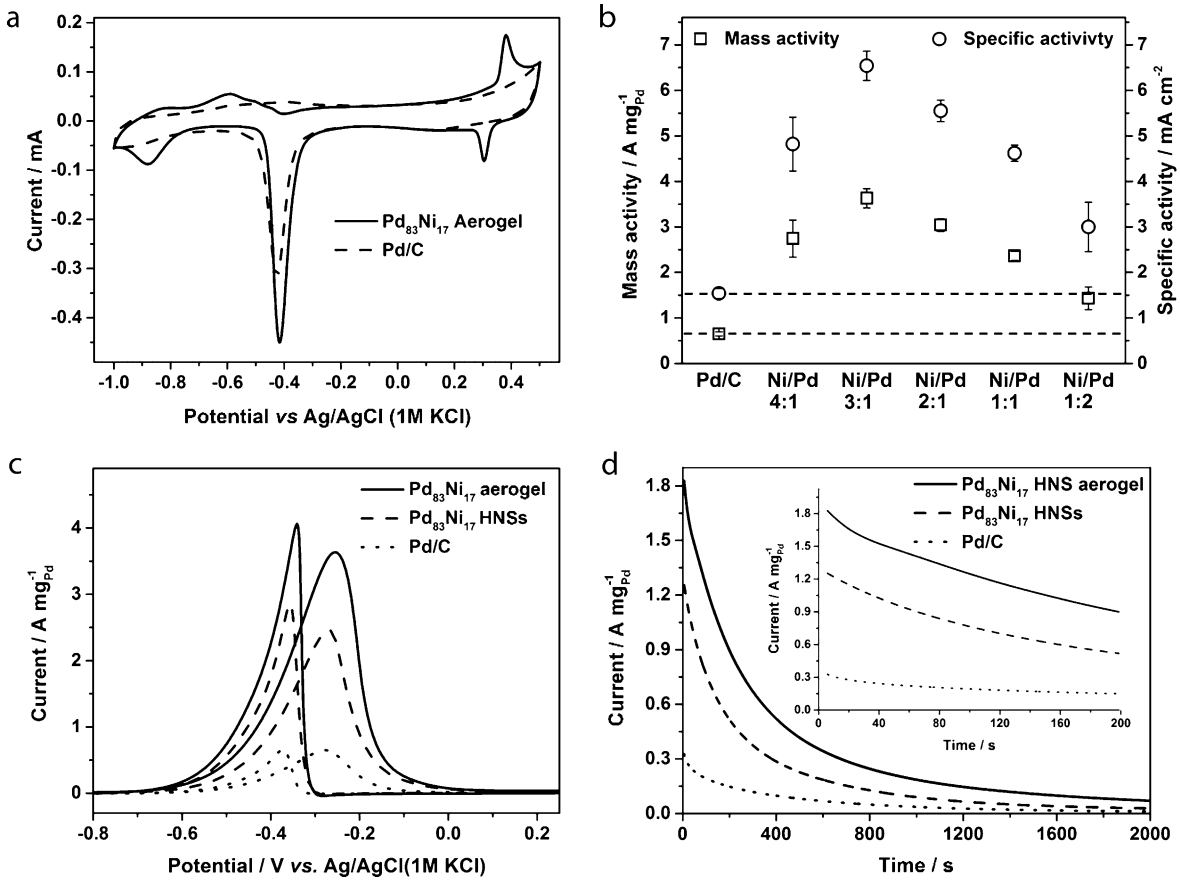

Figure 3. a) Comparison of the CVs of the $Pd_{83}Ni_{17}$ HNS aerogel and commercial Pd/C in N_2-saturated 1 M NaOH solution. Loading of Pd is 20 $\mu g cm^{-2}$. Scan rate: 100 $mV s^{-1}$. b) The mass and specific activities of PdNi HNS aerogels with different Ni/Pd precursor ratios and commercial Pd/C. c) Pd-mass-normalized CVs of the $Pd_{83}Ni_{17}$ HNS aerogel and the $Pd_{83}Ni_{17}$ HNSs in N_2-saturated 1 M NaOH + 1 M ethanol solution. Scan rate: 50 $mV s^{-1}$. d) The Pd-mass-normalized *i–t* curves of the $Pd_{83}Ni_{17}$ HNS aerogel, $Pd_{83}Ni_{17}$ HNSs, and commercial Pd/C in N_2-saturated 1 M NaOH + 1 M ethanol solution.

 © 2015 Wiley-VCH Verlag GmbH & Co. KGaA, Weinheim

efficiency of Pd.[17] As summarized in Figure 3b, the mass activities (MAs) and specific activities (SAs) of the PdNi HNS aerogels are much higher than that of commercial Pd/C. The $Pd_{83}Ni_{17}$ HNS aerogel shows the highest MA (3.63 A mg^{-1}) and SA (6.54 mA cm^{-2}), 5.6 and 4.2 times higher than that of Pd/C (MA: 0.65 A mg^{-1}, SA: 1.54 mA cm^{-2}), respectively. In addition, the fact that the onset potential (Figure S8) of the PdNi HNS aerogels is more negative than that of Pd/C indicates an enhancement in the kinetics of the ethanol oxidation reaction, which represents another crucial parameter for the optimization of an electrocatalyst. To further demonstrate the importance of the 3D network, we compared the MAs and SAs of the aerogel and its building blocks in the case of $Pd_{83}Ni_{17}$ (Figure 3c and Figure S9). The MA is improved by 1.5 times in the 3D network architecture, while the SAs are similar since the chemical properties are the same.

The different activities of the Pd_xNi_y HNS aerogels has been attributed to the difference in the Ni content and the resulting change in morphology. To exclude the morphology interference and investigate the effect of the Ni content, we removed most of the Ni from the $Pd_{83}Ni_{17}$ HNSs by HCl etching and obtaining the $Pd_{96}Ni_4$ HNS aerogel which is labeled $Pd_{96}Ni_4$-HCl (Figure S10). Most of the ECSA survived the HCl etching, indicating the robustness of the HNS aerogel structure (Figure S11a). However, the MA is 28.4% lower and the SA is 24.4% lower than for the Ni-rich HNS aerogels (Figure S11b,c). It is therefore rational to consider an alloying effect with Ni as a great contribution to the activity improvement of our PdNi HNS aerogels. In addition, the hollow architecture of the building blocks accompanied by the aerogel nature confers high porosity and large surface area to the HNS aerogel which facilitates mass transfer and provides more active sites for catalysis. The synergy of the aforementioned effects results in the large activity improvement of the PdNi HNS aerogels, while the self-supportability ensures great durability (no carbon corrosion).[7] The durability of the $Pd_{83}Ni_{17}$ HNS aerogel was tested by chronoamperometry and it reveals higher current density than the $Pd_{83}Ni_{17}$ HNSs and Pd/C (Figure 3d). After the stability test, 95% of the MA of the HNS aerogel could be recovered and the hollow and 3D morphology were mostly retained (Figures S12 and S13).

In summary, we have reported on the function-led design of metallic aerogels, inside which the alloyed PdNi HNS building blocks connect and fuse into a well-defined 3D network. The aerogel nature and the hollow building blocks confer several advantages such as high porosity, large surface area, metallic backbone, and self-supportability upon the PdNi HNS aerogels. These properties facilitate the mass transfer, the exposure of reactive sites, electron transfer, and elimination of support corrosion, which qualify the PdNi HNS aerogels to be promising electrocatalysts. The morphology and shell thickness of the building blocks are strongly dependent on their composition which can be tuned by controlling the Ni/Pd precursor ratios. The $Pd_{83}Ni_{17}$ HNS aerogel exhibits the highest MA and SA values, which are 5.6- and 4.2-fold higher than those of commercial Pd/C. The work highlights the great potential of metallic aerogels as highly efficient electrocatalysts through control of the morphology and composition of the building blocks. This approach may be further generalized for many other electrochemical reactions by the utilization of appropriate metals.

Acknowledgements

We acknowledge support from the European Research Council (ERC-2013-AdG 340419 AEROCAT), the Alexander von Humboldt foundation, and DFG (EY 16/10-2 and EY 16/18-1). We also thank Renate Schulze for the ICP-OES analysis, Susanne Goldberg for the SEM measurements, Christine Damm and Xue Zhao for help with TEM and XPS measurements, and Jan Poppe and Laura Kühn for the help with the electrochemical characterizations.

Keywords: aerogels · electrocatalysis · nanostructures · self-assembly · sol–gel processes

How to cite: *Angew. Chem. Int. Ed.* **2015**, *54*, 13101–13105
Angew. Chem. **2015**, *127*, 13293–13297

[1] W. C. Ren, H. M. Cheng, *Nature* **2013**, *497*, 448.
[2] a) S. S. Kistler, *Nature* **1931**, *127*, 741; b) N. Hüsing, U. Schubert, *Angew. Chem. Int. Ed.* **1998**, *37*, 22; *Angew. Chem.* **1998**, *110*, 22.
[3] a) N. Leventis, N. Chandrasekaran, A. G. Sadekar, C. Sotiriou-Leventis, H. Lu, *J. Am. Chem. Soc.* **2009**, *131*, 4576; b) S. Mahadik-Khanolkar, S. Donthula, A. Bang, C. Wisner, C. Sotiriou-Leventis, N. Leventis, *Chem. Mater.* **2014**, *26*, 1318.
[4] a) J. L. Mohanan, I. U. Arachchige, S. L. Brock, *Science* **2005**, *307*, 397; b) A. Hitihami-Mudiyanselage, K. Senevirathne, S. L. Brock, *ACS Nano* **2013**, *7*, 1163.
[5] a) X. Gao, R. J. Esteves, T. T. Luong, R. Jaini, I. U. Arachchige, *J. Am. Chem. Soc.* **2014**, *136*, 7993; b) K. G. S. Ranmohotti, X. N. Gao, I. U. Arachchige, *Chem. Mater.* **2013**, *25*, 3528.
[6] a) N. Gaponik, A. Wolf, R. Marx, V. Lesnyak, K. Schilling, A. Eychmüller, *Adv. Mater.* **2008**, *20*, 4257; b) N. C. Bigall, A. K. Herrmann, M. Vogel, M. Rose, P. Simon, W. Carrillo-Cabrera, D. Dorfs, S. Kaskel, N. Gaponik, A. Eychmüller, *Angew. Chem. Int. Ed.* **2009**, *48*, 9731; *Angew. Chem.* **2009**, *121*, 9911; c) V. Lesnyak, A. Wolf, A. Dubavik, L. Borchardt, S. V. Voitekhovich, N. Gaponik, S. Kaskel, A. Eychmüller, *J. Am. Chem. Soc.* **2011**, *133*, 13413; d) J. Yuan, D. Wen, N. Gaponik, A. Eychmüller, *Angew. Chem. Int. Ed.* **2013**, *52*, 976; *Angew. Chem.* **2013**, *125*, 1010.
[7] W. Liu, A. K. Herrmann, N. C. Bigall, P. Rodriguez, D. Wen, M. Oezaslan, T. J. Schmidt, N. Gaponik, A. Eychmüller, *Acc. Chem. Res.* **2015**, *48*, 154.
[8] N. Gaponik, A.-K. Herrmann, A. Eychmüller, *J. Phys. Chem. Lett.* **2012**, *3*, 8.
[9] a) W. Liu, P. Rodriguez, L. Borchardt, A. Foelske, J. Yuan, A. K. Herrmann, D. Geiger, Z. Zheng, S. Kaskel, N. Gaponik, R. Kotz, T. J. Schmidt, A. Eychmüller, *Angew. Chem. Int. Ed.* **2013**, *52*, 9849; *Angew. Chem.* **2013**, *125*, 10033; b) D. Wen, A. K. Herrmann, L. Borchardt, F. Simon, W. Liu, S. Kaskel, A. Eychmüller, *J. Am. Chem. Soc.* **2014**, *136*, 2727.
[10] Y. J. Wang, N. Zhao, B. Fang, H. Li, X. T. Bi, H. Wang, *Chem. Rev.* **2015**, *115*, 3433.
[11] a) X. Xia, Y. Wang, A. Ruditskiy, Y. Xia, *Adv. Mater.* **2013**, *25*, 6313; b) V. R. Stamenkovic, B. Fowler, B. S. Mun, G. Wang, P. N. Ross, C. A. Lucas, N. M. Markovic, *Science* **2007**, *315*, 493.
[12] C. Baldizzone, S. Mezzavilla, H. W. Carvalho, J. C. Meier, A. K. Schuppert, M. Heggen, C. Galeano, J. D. Grunwaldt, F. Schuth,

 © 2015 Wiley-VCH Verlag GmbH & Co. KGaA, Weinheim

K. J. Mayrhofer, *Angew. Chem. Int. Ed.* **2014**, *53*, 14250; *Angew. Chem.* **2014**, *126*, 14474.
[13] W. Liu, A. K. Herrmann, D. Geiger, L. Borchardt, F. Simon, S. Kaskel, N. Gaponik, A. Eychmüller, *Angew. Chem. Int. Ed.* **2012**, *51*, 5743; *Angew. Chem.* **2012**, *124*, 5841.
[14] S. Guo, S. Zhang, S. Sun, *Angew. Chem. Int. Ed.* **2013**, *52*, 8526; *Angew. Chem.* **2013**, *125*, 8686.
[15] B. Y. Xia, H. B. Wu, N. Li, Y. Yan, X. W. Lou, X. Wang, *Angew. Chem. Int. Ed.* **2015**, *54*, 3797; *Angew. Chem.* **2015**, *127*, 3868.
[16] L. Xiao, L. Zhuang, Y. Liu, J. Lu, H. D. Abruna, *J. Am. Chem. Soc.* **2009**, *131*, 602.
[17] X. Zhao, S. Chen, Z. Fang, J. Ding, W. Sang, Y. Wang, J. Zhao, Z. Peng, J. Zeng, *J. Am. Chem. Soc.* **2015**, *137*, 2804.

Received: June 10, 2015
Revised: July 10, 2015
Published online: September 10, 2015

 © 2015 Wiley-VCH Verlag GmbH & Co. KGaA, Weinheim